



Research paper

A subunit of V-ATPases, ATP6V1B2, underlies the pathology of intellectual disability



Weihao Zhao^{a,b,1}, Xue Gao^{a,c,1}, Shiwei Qiu^{a,1}, Bo Gao^a, Song Gao^a, Xin Zhang^a, Dongyang Kang^a, Weiju Han^{a,*}, Pu Dai^{a,*}, Yongyi Yuan^{a,*}

^a Department of Otolaryngology, Head and Neck Surgery, Chinese PLA General Hospital, 28# Fuxing Road, Beijing 100853, China

^b Department of Otolaryngology General Hospital of Tibet Military Region, Lhasa 850007, China

^c Department of Otolaryngology, PLA Rocket Force Characteristic Medical Center, 16# XinWai Da Jie, Beijing 100088, China

ARTICLE INFO

Article history:

Received 22 April 2019

Received in revised form 6 June 2019

Accepted 18 June 2019

Available online 27 June 2019

Keywords:

Dominant deafness-onychodystrophy (DDOD) syndrome

ATP6V1B2

V-ATPases

Cognitive defects

ABSTRACT

Background: Dominant deafness-onychodystrophy (DDOD) syndrome is a rare disorder mainly characterized by severe deafness, onychodystrophy and brachydactyly. We previously identified c.1516C > T (p.Arg506X) in *ATP6V1B2* as cause of DDOD syndrome, accounting for all cases of this genetic disorder. Clinical follow-up of DDOD syndrome patients with cochlear implantation revealed the language rehabilitation was unsatisfactory although the implanted cochlea worked well, which indicates there might be learning and memory problems in DDOD syndrome patients. However, the underlying mechanisms were unknown.

Methods: *atp6v1b2* knockdown zebrafish and *Atp6v1b2* c.1516C > T knockin mice were constructed to explore the phenotypes and related mechanism. In mutant mice, auditory brainstem response test and cochlear morphology analysis were performed to evaluate the auditory function. Behavioral tests were used to investigate various behavioral and cognitive domains. Resting-state functional magnetic resonance imaging was used to evaluate functional connectivity in the mouse brain. Immunofluorescence, Western blot, and co-immunoprecipitation were performed to examine the expression and interactions between the subunits of V-ATPases.

Findings: *atp6v1b2* knockdown zebrafish showed developmental defects in multiple organs and systems. However, *Atp6v1b2* c.1516C > T knockin mice displayed obvious cognitive defects but normal hearing and cochlear morphology. Impaired hippocampal CA1 region and weaker interaction between the V1E and B2 subunits in *Atp6v1b2*^{Arg506X/Arg506X} mice were observed.

Interpretation: Our study extends the phenotypic range of DDOD syndrome. The impaired hippocampal CA1 region may be the pathological basis of the behavioral defects in mutant mice. The molecular mechanism underlying V-ATPases dysfunction involves a weak interaction between subunits, although the assembly of V-ATPases can still take place.

© 2019 Published by Elsevier B.V. This is an open access article under the CC BY-NC-ND license (<http://creativecommons.org/licenses/by-nc-nd/4.0/>).

1. Introduction

ATP6V1B2 encodes the B2 subunit in V-ATPases, a multisubunit protein complex consisting of a soluble V1 subcomplex (responsible for hydrolyzing ATP) and a membrane-bound V0 subcomplex (involved in H⁺ translocation) expressed in virtually all eukaryotes. V1 is composed of eight different subunits (A–H). Three pairs of A and B subunits constitute a sexangular head of the V1 complex, and AB pairs can undergo conformational changes to bind ATP, ADP, and phosphate. A central rotational stalk made of subunits D and F and a peripheral stationary shaft made

of subunits C, E, G, and H both join the V1 complex and the V0 complex. The proton-transporting V0 complex is composed of six subunits (a, d, e, c, c', and c''). The central rotational stalk made of the D and F subunits extends to the ring of subunit c via the d subunit. V1 and V0 reversibly dissociate in a few species, including mammals [1–3]. V-ATPases establish and maintain an acidic environment by pumping protons into the lumen, a process that requires ATP hydrolysis [4]. As proton pumps are present in the membranes of intracellular organelles, such as dictyosomes, endosomes, lysosomes, and synaptic vesicles, wherein acidification is vital, V-ATPases are very important for the development of multicellular life [5], and for multiple cellular functions including vesicular trafficking, lysosome degradation, and acidification of intracellular organelles [4,6,7]. Accordingly, V-ATPases has been implicated in a number of diseases, including neurodegeneration [8], cutis laxa [9], bone disease [10], cancer [11], renal disease, and deafness [12]. There exist two highly

* Corresponding authors.

E-mail addresses: hanweiju@aliyun.com (W. Han), daipu301@vip.sina.com (P. Dai), yyymzh@163.com (Y. Yuan).

¹ Weihao Zhao, Xue Gao, Shiwei Qiu contributed equally to this paper.

Research in context

Evidence before this study

ATP6V1B2 c.1516C > T (p.Arg506X) was verified to underlie the pathogenesis of dominant deafness-onychodystrophy (DDOD) syndrome by our group. Clinical follow-up of DDOD patients revealed the language rehabilitation was not satisfactory although the implanted cochlea worked well and the hearing loss could get effective compensation, which indicates there might be subtle learning and memory problems in DDOD patients. Although several studies have suggested possible association between *ATP6V1B2* and central nervous system (CNS) disorders like Alzheimer's disease, depression and seizures in human, no CNS disorders are recorded in DDOD, the underlying mechanisms were largely unknown.

The value of this study

We created two genetic models and verified that a defect in *Atp6v1b2* causes CNS disorders. Phenotypic analysis of the zebrafish model suggests that *atp6v1b2* impairment affects early development. The fact that *Atp6v1b2* c.1516C > T knockin mice exhibit decreased expression of *Atp6v1b2*, despite their normal hearing and cochlear morphology, suggests the existence of a compensatory mechanism in the inner ear, although this requires further investigation. Additionally, the impaired hippocampal CA1 region may be the pathological basis of the behavioral defects seen in *Atp6v1b2*^{Arg506X/Arg506X} mice. The molecular mechanism underlying V-ATPases dysfunction involves a weak interaction between the E and B2 subunits, although the assembly of V-ATPases can still take place.

Implications of all the available evidence

The results extend the phenotype range of DDOD syndrome and are helpful to a full recognition on the function of *ATP6V1B2* in CNS and the development of future therapeutic interventions.

homologous isoforms of the B subunit (56 kDa) of V-ATPases in mammals: B1 (encoded by *ATP6V1B1*) and B2. Both the B1 and B2 subunits are crucial for assembly of the V-ATPases [13,14], and for the interaction between V-ATPases and actin filaments [15]. In mammals, subunits B1 and B2 show different expression patterns. The B2 isoform, also termed as the brain isoform, is ubiquitous [16], while the B1 isoform is detected exclusively in the kidney, epididymis, eyes, and inner ears [17–20]. Interestingly, the B2 subunit can substitute B1 subunit function by relocalizing B2-containing V-ATPases [21].

ATP6V1B1 is associated with distal renal tubular acidosis (dRTA, MIM: 602722), a rare disease characterized by metabolic acidosis and sensorineural deafness [12], while *ATP6V1B2* is the disease-causing gene of dominant deafness-onychodystrophy syndrome (DDOD syndrome, MIM: 124480) and Zimmermann-Laband syndrome (ZLS, MIM: 135500). DDOD syndrome, which forms the backdrop of the current study, is an autosomal dominant genetic disease that leads to severe congenital sensorineural deafness, absence of nails and/or toes, the presence of pointed teeth in some cases, onychodystrophy, and brachydactyly. We previously identified one de novo pathogenic variant (c.1516C > T (p.Arg506X)) in *ATP6V1B2* as the molecular pathogenesis of DDOD syndrome, which leads to V-ATPases dysfunction and abnormal lysosome acidification [22]. One current clinical case report also confirmed that *ATP6V1B2* c.1516C > T (p.Arg506X) causes DDOD syndrome [23].

ATP6V1B2 variant is also associated with ZLS, a developmental disorder characterized by facial dysmorphism characterized by gingival enlargement, intellectual disability, hypoplasia or aplasia of the nails and terminal phalanges, and hypertrichosis. DDOD and ZLS share the phenotypes of nail and phalangeal aplasia. *ATP6V1B2* c.1516C > T in all DDOD families, and c.1454 G > C in several ZLS families, both arose *de novo*²⁴.

Intellectual disability and seizures are rarely reported in DDOD syndrome, unlike ZLS syndrome. However, several studies have suggested an association between *ATP6V1B2* and central nervous system (CNS) disorders, although it is unclear how *ATP6V1B2* is involved in such symptoms. For example, using a mouse model, a previous study demonstrated that *Atp6v1b2* is involved in synaptic transmission and related to Alzheimer's disease [25]. Genetic linkage analysis of five French families revealed *ATP6V1B2* as one of the candidate genes of generalized epilepsy with febrile seizures plus [26]. A recent genome-wide association study suggested that the *ATP6V1B2* rs1106634 A allele is associated with a lifetime risk of depression and hippocampal cognitive deficits [27].

To date, 10 DDOD syndrome patients have been reported and all presented with severe congenital sensorineural deafness [22,23]. Since neurological and behavioral problems are ubiquitous in deaf individual [28], preexisting mild CNS disorders may be neglected in subjects with DDOD syndrome. We have observed unsatisfactory speech rehabilitation in one patient with DDOD syndrome 7 years after cochlear implantation, and this patient underwent regular postoperative cochlea mapping and speech training. The cochlea mapping results indicated that the implanted cochlea worked well as evaluated by the threshold level (T level), comfortable level (C level), and dynamic range (DR), which are the principle assessment indicators for cochlear implants. Therefore, the poor speech rehabilitation was considered to be associated with learning or memory problems. In a recently collected DDOD syndrome pedigree, the mother (21 years old) was diagnosed with mild intellectual disorder using the Hastgawa Dementia Scale with a score of 29 (the normal value should be >31), while her 17-month-old son presented with a mental age of 9 months according to the results of the Denver developmental screening test administered by paediatric neurological physicians. Therefore, it is important to elucidate the underlying pathogenesis of c.1516C > T related CNS disorders in DDOD syndrome. Here, we created and analyzed two genetic models: one is *atp6v1b2* knockdown zebrafish and the other is *Atp6v1b2* c.1516C > T knockin mice. We show that (1) *atp6v1b2* knockdown zebrafish have developmental defects in multiple organs and systems; (2) *Atp6v1b2* c.1516C > T knockin mice display cognitive disorders, and the impaired hippocampal CA1 region may be the pathological basis; (3) the normal hearing thresholds of *Atp6v1b2* c.1516C > T knockin mice of 24 weeks old suggest the existence of compensation mechanism in the auditory system; and (4) V-ATPases assembly still occurs in *Atp6v1b2* c.1516C > T, but the interaction between the E and B2 subunits is weak compared to wild-type (WT). Our study confirms that defective *Atp6v1b2* leads to CNS impairments, extends the phenotype range of DDOD syndrome, and is helpful to a full recognition on the function of *ATP6V1B2*.

2. Materials and methods

2.1. Ethics statement

All in vivo experiments were carried out in accordance with CALAS (Chinese Association for Laboratory Animal Science) guidelines for the care and use of laboratory animals and were approved by the Animal Care and Use Committees of the Chinese PLA General Hospital and the Shanghai Biomodel Organism Science & Technology Development Co. Ltd.

2.2. *Atp6v1b2* knockdown zebrafish

AB strain zebrafish were used and maintained under standard conditions [29]. Embryos were staged as previously described [30]. Antisense

Morpholino (MO) was microinjected into fertilized one-cell-stage embryos using a standard protocol [31]. The sequence of the *atp6v1b2* splice-blocking MO was 5'- ATGTTTTTCTAAATCTCACCCAGC-3' (E4I4-MO, Gene Tools). For the *atp6v1b2* gene knockdown experiment, 4 ng of control-MO or *atp6v1b2-e4i4*-MO (E4I4-MO) were used per injection.

2.3. DASPEI staining of lateral line hair cells

After microinjection, larvae (5 dpf) were immersed in 1 mM DASPEI (2-(4-(dimethylamino)styryl)-N-ethylpyridinium iodide, Sigma) in fish water for 1 h, anesthetized with 0.016% (w/v) tricaine methanesulfonate (TMS) (MS-222, Sigma), oriented laterally (anterior, left; posterior, right; dorsal, top), and mounted (using methylcellulose) in a depression slide prior to fluorescence microscopy. Hair cells stereotypically located on the lateral line were stained as green dots.

2.4. Data acquisition and analysis

Embryos and larvae were analyzed using a Nikon SMZ 1500 fluorescence microscope, and photographed with a digital camera. Quantitative image analysis was performed with the aid of image-based morphometric (NIS-Elements D3.1, Japan) and ImageJ software (United States National Institutes of Health; <http://rsbweb.nih.gov/ij/>). Lateral line hair cells were quantified (particle numbers) with ImageJ software. Ten fish were subjected to each treatment, and signal numbers/fish were calculated by data averaging.

2.5. *Atp6v1b2* knockin mice

Atp6v1b2 c.1516C > T knockin mice were generated by Shanghai Model Organisms Center, Inc. (Shanghai, China). An *Atp6v1b2*-targeting vector was constructed by ET cloning techniques in EL250 bacterial cells [32]. The targeting vector contained a 3 kb 5' homology arm, a pGK-Neomycine-polyA drug positive selection cassette, an *Atp6v1b2* mutation site, and a 3.4 kb 3' homology arm. The targeting vector was electroporated into a mouse embryonic stem cell (ES) line with a C57BL/6 (Agouti) background. After drug selection with G418, the resistant ES clones were identified by long PCR and confirmed by sequencing. The primers used for genotyping to confirm that the homologous recombination occurred correctly. The primers used for genotyping the correct homology recombination were 5'- CTATCGAGAAGGAATGAC CAG-3' and 5'- AAGGGACAGGAATGAAAGAAAC-3' for the correct 5' homology arm recombination and 5'-TCGCATTGTCTGAGTAGGTGTC-3' and 5'- TCTTACCTCTAAGCAAATC-3' for the correct 3' homology arm recombination. Four Positive ES cell clones were identified and injected into C57BL/6 blastocysts to generate the chimeric offspring. The chimeric mice were mated with C57BL/6 J mice to obtain the *Atp6v1b2* heterozygous knock-in mice. The heterozygous mice were crossed to obtain the *Atp6v1b2* homozygous point mutation mice. The genotypes of the offspring mice were identified by PCR. The primers were 5'- CACTCAATAAAACCCTGTCTTAAA -3' and 5'- GTCTCGTGAC ATGGACAGCACCG-3', and the PCR products were confirmed by direct sequencing.

Mice body weights were recorded at 8 weeks [WT: male $n = 7$, female $n = 5$; *Atp6v1b2*^{Arg506X/+} heterozygote (HE): male $n = 7$, female $n = 5$; *Atp6v1b2*^{Arg506X/Arg506X} homozygote (HO): male $n = 5$, female $n = 5$], 16 weeks (WT: male $n = 5$, female $n = 6$; HE: male $n = 8$, female $n = 6$; HO: male $n = 6$, female $n = 5$), 24 weeks (WT: male $n = 8$, female $n = 8$; HE: male $n = 14$, female $n = 11$; HO: male $n = 9$, female $n = 6$), and 32 weeks (WT: male $n = 7$, female $n = 6$; HE: male $n = 13$, female $n = 9$; HO: male $n = 7$, female $n = 5$).

2.6. Auditory brainstem responses (ABR)

Hearing was evaluated in WT and mutant mice. ABR were registered in 16- and 24-week-old mice ($n =$ number of test ears; 16 weeks: $n = 10$ /group; 24 weeks: HO: $n = 11$, WT: $n = 8$). In brief, ABR recordings were obtained under anesthesia with an intraperitoneal injection of 1% sodium pentobarbital (10 ml/kg) and the body temperature was maintained at 37 °C with a thermal blanket. Needle electrodes were placed subdermally at the base of the ears (the active electrode and the grounding electrode) and the vertex of the cranium (the reference electrode). Interelectrode impedances were kept below 1k Ω . The signal was filtered (100–3000 Hz), amplified ($\times 50,000$), and averaged using TDT III hardware and SigGen/Biosig software. The electrical responses were recorded averagely, and hearing thresholds were determined in the ABR recordings. The stimuli included click and tone burst (2, 4, 8, 16, 24, and 32 kHz) and were presented from 90 to 10 dB. The ABR threshold was defined as the lowest intensity that elicited a detectable response reliably (an identifiable waveform can be seen).

2.7. Behavioral assays

All behavioral tests were carried out in an independent and quiet room. 12-week-old animals (male: WT $n = 10$, HE $n = 11$, HO $n = 10$) were placed 30 min in advance for acclimatization before testing. All instruments were cleaned up when one mouse had been moved out.

Open-field test: Open-field test reflects anxiety-like behavior based on thigmotaxis in mice [33]. Mice were placed in the open field (Kinder Scientific Company LLC) and monitored for 15 min, each mouse entered at the same position. The distance and time at center/edge regions were recorded and compared. The center-edge-ratio was used to determine anxiety. Anxious mice are expected to spend less time exploring center regions.

Elevated Plus Maze (EPM): EPM is a reliable measurement tool to investigate anxiety-related defensive behaviors in mice. EPM consists of two open arms and two closed arms (25 cm \times 8 cm \times 12 cm). The elevated plus maze was placed on a movable platform with casters 50 cm off the ground. Mouse was placed at the junction (8 cm \times 8 cm) and faced the same open arm. A camera hung above the junction was used to record mouse activity time and distance in open or closed arms. EPM intuitively reflected the anxious state. The distance and time at open and closed arms were recorded and compared. Anxious mice are expected to spend less time exploring open arms.

Light-dark Exploration Test (LDT): LDT measured anxiety-like behavior. LDT apparatus consists of two perspex boxes (Kinder Scientific Company LLC), an open white compartment (16 cm \times 16 cm \times 16 cm) brightly illuminated by a 100 W desk lamp, and a dark compartment (16 cm \times 16 cm \times 16 cm) covered with black perspex top. An aperture (8 cm \times 5 cm) at floor level exists between the two compartments. Mice were individually placed near the aperture facing the dark compartment and allowed to freely explore the apparatus for 15 min. The trajectory of mice was recorded by infrared detection and transmitted to the system software (KS motor monitor) for analysis. The activity time of mice in bright field and dark field was analyzed. Anxious mice are expected to spend less time exploring bright region.

Morris Water Maze (MWM): MWM is the most common test used to evaluate cognitive functions related with memory. Spatial memory in the MWM was assessed in a circular pool (diameter: 1.5 m, depth: 25 cm) filled with water (23 \pm 1 °C). However, in this study, MWM test failed to proceed because epilepsy symptoms were induced as *Atp6v1b2*^{Arg506X/Arg506X} mice entered the water.

New Object Recognition Test (NOR): NOR was used to assess the learning and memory ability of mice. NOR was assessed in a black perspex box (32 cm \times 16 cm \times 16 cm). Day 1: Adaptation period; Day 2: The mouse was placed between two same building blocks and allowed to freely explore the apparatus for 15 min. Then the mouse was

returned to the home cage, and a building block was replaced by a totally new one. Four hours later, the mouse was placed between the two building blocks and allowed to explore the apparatus for 10 min. Then the mouse was returned to the home cage. Day 3: One old building block was placed by a totally new one, and the mouse was allowed to explore the apparatus for 10 min. The time spent investigating the objects in the first 5 min was assessed. Mice with learning and memory impairment are supposed to spend less time exploring new blocks than normal mice.

Passive Avoidance Test (PAT): PAT was used to determine learning and memory ability of the mice. Day 1: The mouse was placed in the bright compartment. After 30 s, the door to the dark compartment was opened to allow the mouse to explore the apparatus freely for 5 min. The time mouse spent to completely enter the dark compartment was recorded as a latency time of Day 1. Day 2: 30 s later after the mouse was placed in the bright compartment, the door was opened. Next, the door was closed until mouse extremities completely entered the dark compartment. Then the mouse was punished by a mild foot-shock (2 s, 0.5 mA). The mouse was returned to the home cage 30 s later. The time mouse spent to completely enter the dark compartment was recorded as a latency time of Day 2. Day 3: The mouse was placed in the bright compartment. 5 s later the door to the dark compartment was opened, and no foot-shock was given. The time mouse spent to completely enter the dark compartment was recorded as a latency time of Day 3. The latency time of WT, HO, and HE groups was compared. Mice with learning and memory impairment are supposed to have shorter latency time than normal on the third day.

2.8. Resting-state functional MRI

Resting-state functional MRI (rsfMRI) was used to evaluate functional connectivity (FC) in the mouse brain. Fourteen 12-week-old mice (male: WT, $n = 7$; HO, $n = 7$) underwent rsfMRI. Before MRI scanning, the mice were initially anesthetized using 3–4% oxygen enriched isoflurane following with 1.5% oxygen enriched isoflurane during scanning. The effects on blood oxygen level-dependent (BOLD) signals of respiration and heartbeat were inevitable. To reduce the impact of physiological activities, mice were placed in a prone position with their head placed firmly in a tooth bar and ear bar. The physiological conditions including respiration rate and body temperature were monitored (SA Instruments, Stony Brook, NY, USA). The core body temperature was controlled to 37 °C using a controlled warm air system (Thermo Scientific SC100, Waltham, MA, USA). MRI data were acquired and analyzed at the Center for Advanced Imaging, Institute of Automation, Chinese Academy of Sciences using a Biospec 94/30 preclinical system (Bruker BioSpin GmbH, Ettlingen, Germany) operating at 400 MHz (9.4 T) equipped with a gradient coil of 12 cm inner diameter and a maximum gradient strength of 660 mT/m.

Data collection: T2-weighted anatomical scan was acquired using 2D TurboRARE (turbo rapid acquisition with relaxation enhancement) sequence with the following parameters: field of view (FOV) $20 \times 20 \text{ mm}^2$, matrix 256×256 , slice thickness 0.2 mm, repetition time (TR) 8896 ms, echo time (TE) 33 ms, flip angle (FA) 90°, bandwidth 35 kHz, RARE factor 8, and number of averages (NEX) 1. rsfMRI imaging was recorded using 2D T2star-FID-EPI sequence with the following parameters: field of view (FOV) $35 \times 9 \text{ mm}^2$, matrix 117×30 , slice thickness 0.3 mm, repetition time (TR) 2000 ms, echo time (TE) 4.9 ms, flip angle (FA) 90°, bandwidth 450 kHz, and number of averages (NEX) 1. The reconstructed images have an isotropic voxel size of 300 μm .

Data analysis: Brain volumes were compared between *Atp6v1b2*^{Arg506X/Arg506X} and WT mice and the voxel-based morphometry was on T2-weighted anatomical images. Regions-of-interest (ROI) were defined according to WHS mouse brain atlas. Modulated gray matter segmentation was used to calculate volumes of the ROIs. In total, 54 ROIs (27 on each hemisphere) out of the 78 ROIs in the atlas were included for calculation (Fig. S1). And brain regions with different

functional connections were selected for mapping. Additionally, we compared group differences in the functional connections between hippocampus, amygdala (seeds), and cortex (target). The cluster size threshold is 0.1 mm^3 .

SPM8 software with in-house Matlab scripts was used to do the pre-processing of the rsfMRI data including slice timing correction, head motion correction, normalization and smoothing. Motion correction was performed by realignment and motion regression. During pre-processing, a two-pass realignment was used; that is, all image volumes were first realigned to the average volume, and then, the average volume of the resultant realigned images was computed, to which images were aligned again. For general linear model (GLM) analysis, motion-related components from the data were removed by taking the calculated motion parameters as regressors (e.g. six nuisance regressors corresponding to three translation and three rotation parameters). For each region of interest (ROI), time courses of its voxels were extracted and averaged over the ROI. Nuisance covariates associated with the estimated head-motion parameters were regressed out. The pairwise functional connectivity (FC) between ROIs was computed as the Pearson's correlation coefficient between the pre-processed blood oxygen level-dependent (BOLD) signals. To improve the normality of the coefficients, a Fisher's z transformation was applied. For each FC, a one-sample t -test against zero was performed, and FCs that passed the test ($p < 0.05$) were taken for further analysis. Multiple group comparisons were corrected for the false discovery rate (FDR) ($p < 0.05$).

2.9. Immunocytochemistry

Antibodies used were as follows: primary antibodies, polyclonal rabbit anti-ATP6V1B2 (Abcam, UK, ab73404), monoclonal rat anti-LAMP1 (Abcam, UK, ab25245), monoclonal mouse anti-NeuN, clone A60 (Millipore, USA, MAB377). Secondary antibodies, Alexa Fluor 488 Goat Anti-rabbit IgG (H + L) (Lifetechnologies, USA, A11008), Alexa Fluor 568 Goat Anti-Rat IgG (H + L) (Lifetechnologies, USA, A11077), Alexa Fluor 568 Goat Anti-Mouse IgG (H + L) (Lifetechnologies, USA, A11004). Adult mice were deeply anesthetized with an intraperitoneal injection of 1% sodium pentobarbital (10 ml/kg) and perfused with 0.9% NaCl solution followed by 4% paraformaldehyde.

Cochlea: for cryosections, the cochleas of 16 or 24 weeks old mice were harvested quickly from the temporal bone and fixed with 4% PFA, decalcified, dehydrated with a graded series of ethanol; serial sections were cut at 10- μm thickness. The sections were incubated with primary antibody (diluted with PBS, 1:500) at 4 °C overnight and with secondary antibodies (diluted with PBS, 1:500) at 37 °C for 2 h. The nuclei were labelled with DAPI (4',6-diamidino-2-phenylindole, 1 \times , ZSJB-Bio, Beijing, China). Images were captured with a digital camera mounted on Zeiss confocal microscope (LSM780). Hematoxylin/Eosin (H&E) staining of cochlea: tissues were stained with hematoxylin-eosin and images were acquired using an optical microscope (OLYMPUS, BX51). Slides spanning the entire inner ear from three different mice were stained, and the observed expression patterns were considered reliable if present in all three samples. The primary antibody was omitted as a control.

Brain: the brains of 12 weeks old mice were removed from the skulls and post-fixed in 4% paraformaldehyde for 24 h at 4 °C, dehydrated with a graded series of ethanol; Serial sections were cut at 20- μm thickness. The sections were placed in solution (37 °C, 100 μl goat serum + 50 μl 10% TritonX-100 + 850 μl PBS) for 20 min. Then the sections were incubated with primary antibody (diluted with PBS, 1:500) at 4 °C overnight and incubated with secondary antibodies (diluted with PBS, 1:500) at 37 °C for 2 h. The nuclei were labelled with DAPI (1 \times , ZSJB-Bio, Beijing, China). Images were captured with a digital camera mounted on Zeiss confocal microscope (LSM780). ImageJ was used for cell counters. Samples (WT: 20 slices, HE: 14 slices, HO: 19 slices) at same level were selected for cell counters. The primary antibody was omitted as a control.

2.10. Western blot

For Western blot analysis, hippocampus and cochlea from WT and mutant mice were removed and protein was extracted (hippocampus from 12 weeks old mice, cochlea from 16 weeks old mice). Then equal amounts of protein sample were separated on a 12% Tris/Glycine SDS-PAGE (Applygen Technologies Inc.B1027) and transferred to polyvinylidene difluoride membrane. Primary antibodies were the same as immunofluorescence (diluted with TBST, 1:1000, at 4 °C overnight). The experiments were independently repeated for three times.

2.11. Co-immunoprecipitation

Primary antibodies used in experiment included polyclonal rabbit anti-ATP6V1B2 (Abcam, UK, ab73404), Anti-ATP6V1E2 (Abcam, UK, ab126186), Anti-ATP6V1A (Abcam, UK, ab137574), and Anti-ATP6V0B (Abcam, UK, ab107189). Co-immunoprecipitation was independently biologically repeated three times to appropriately control the Western blot analysis. We removed the hippocampus and cochlea quickly from the mice skull and added 100 μ l Co-IP lysis buffer for the cochlea and 500 μ l for the hippocampus. The samples were centrifuged for 20 min at a speed of 14,000 r.p.m. to obtain the supernatant containing the antigen. Then, the antigen-antibody complex was formed by incubating polyclonal rabbit anti-ATP6V1B2 antibody with the antigen-containing supernatant overnight at 4 °C. Next, we followed the instructions for Pierce Protein A/G Magnetic Beads (<https://www.thermofisher.com/order/catalog/product/88802>) to obtain the samples containing the antigen-antibody complex. Finally, loading buffer was added to the samples containing the antigen-antibody complex followed by Western blotting analysis. Atp6v1b2 was used as a reference in this experiment. As the expression of Atp6v1b2 was lower in *Atp6v1b2*^{Arg506X/Arg506X} mice than in the WT mice, the number of the samples from each group for Co-IP was adjusted to ensure equal levels of Atp6v1b2 as a reference protein.

The normalised fluorescence intensities were compared between the *Atp6v1b2*^{Arg506X/Arg506X} and WT groups. For Co-IP, the normalised fluorescence intensity was defined as the ratio of the gray value of other subunits to the gray value of Atp6v1b2. Comparisons between the *Atp6v1b2*^{Arg506X/Arg506X} and WT groups were analyzed by Student's *t*-test. **P* < 0.05 (***P* < 0.01) was considered to indicate a statistically significant difference.

2.12. Statistical analysis

SPSS 13.0 (SPSS, Inc., Chicago, IL, USA) was used for statistical analysis and data was expressed as the mean \pm standard deviation. Comparisons between HO and WT were analyzed by Student's *t*-test, and one-way ANOVA with Student-Newman-Keuls test was used for multiple comparisons (between HO, HE, and WT). Statistical significance is indicated as **P* < 0.05 and ***P* < 0.01. ImageJ was used for cell counters.

3. Results

3.1. *atp6v1b2* knockdown causes developmental defects in zebrafish

The zebrafish *atp6v1b2* gene was targeted by a specific MO antisense strategy to prevent proper splicing of exon 4 (E4I4-MO). *Atp6v1b2*-e4i4-MO was active, as confirmed by RT-PCR (Fig. 1a).

Zebrafish injected with *atp6v1b2* E4I4-MO (4 ng) showed altered phenotypes. Compared to WT, *atp6v1b2* knockdown zebrafish had a shorter body length, smaller-sized brain ventricles, severe pericardial edema, a non-inflated swim bladder, shorter pectoral fins, and hair cell loss (Fig. 1b–e).

3.2. General appearance of *Atp6v1b2* c.1516C > T knockin mice

The primer's location was noted in the Fig. 2a. Knockin of the *Atp6v1b2* c.1516C > T variant was confirmed by PCR of mouse tail DNA (Fig. 2b). As a characteristic manifestation of systemic health and development, the body weights of *Atp6v1b2*^{Arg506X/Arg506X}, *Atp6v1b2*^{Arg506X/+}, and WT mice were compared, and the difference were obvious at 16 weeks (Fig. 2c, d). Reduced body weight is a characteristic of the *Atp6v1b2* c.1516C > T knockin mouse model. In contrast to WT and *Atp6v1b2*^{Arg506X/+} mice, there was less body weight gain in *Atp6v1b2*^{Arg506X/Arg506X} mice with increased age independent of gender, thus leading to significantly lower body weight in older *Atp6v1b2*^{Arg506X/Arg506X} mice (one-way analysis of variance, **P* < 0.05, ***P* < 0.01).

3.3. The c.1516C > T knockin mice display normal hearing before 24 weeks

We aimed to explore the cause of hearing loss in DDOD syndrome by studying auditory function and cochlear morphology in the *Atp6v1b2* c.1516C > T knockin mice. However, *Atp6v1b2* c.1516C > T knockin mice did not display abnormal mean hearing thresholds, as demonstrated by the auditory brainstem response test at 16 and 24 weeks (Fig. 3a).

3.4. *Atp6v1b2*^{Arg506X/Arg506X} cochleas express less *Atp6v1b2* than WT despite a normal morphology and expression pattern

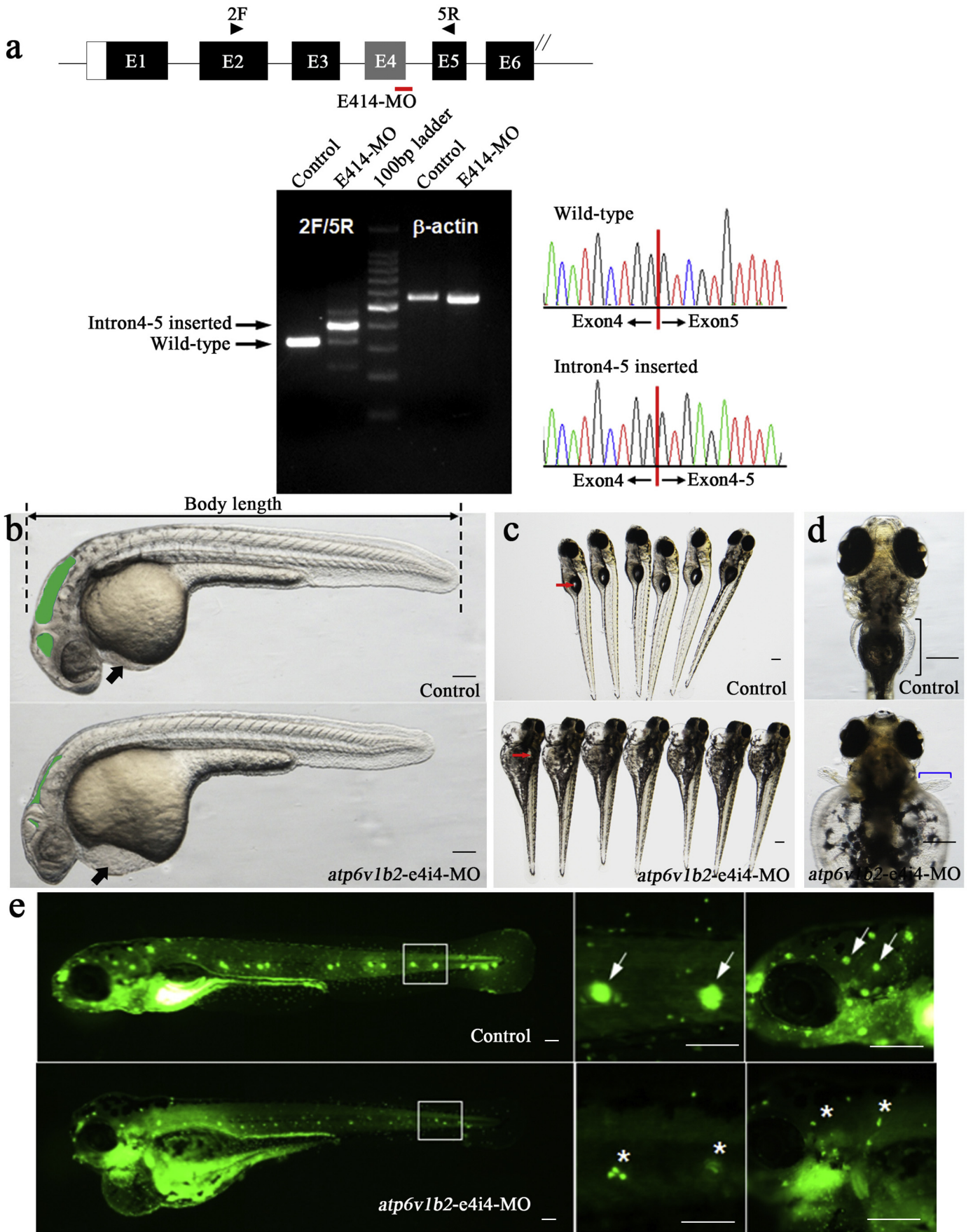
Morphologic analysis of the inner ear of *Atp6v1b2* c.1516C > T knockin mice appeared normal (Fig. 3c). Immunofluorescence analysis showed that Atp6v1b2 was expressed ubiquitously in both WT and *Atp6v1b2*^{Arg506X/Arg506X} inner ears, and highly expressed in spiral ganglion and the organ of Corti especially inner hair cells (Fig. 3b). V-ATPases deficits can cause lysosomal storage diseases and the appearance of enlarged lysosomes [34]. An anti-Lamp1 antibody was used to mark lysosomes and no abnormalities were observed. Western blot analysis revealed that the expression level of Atp6v1b2 in *Atp6v1b2*^{Arg506X/Arg506X} cochlea was significantly lower than WT (Fig. 3d). Consistent with the immunofluorescence analysis, the expression of Lamp1 showed no significant difference between *Atp6v1b2*^{Arg506X/Arg506X} and WT cochleas.

3.5. Behavioral changes and cognitive deficits in *Atp6v1b2* c.1516C > T knockin mice

NOR and PAT were used to examine learning and memory abilities of the mice. WT mice performed better than *Atp6v1b2*^{Arg506X/+} and *Atp6v1b2*^{Arg506X/Arg506X} mice (Fig. 4a, b). In the NOR test, WT mice spent significantly more time on the new block than the old block. However, the time spent exploring the new and old blocks did not differ in the *Atp6v1b2*^{Arg506X/+} or *Atp6v1b2*^{Arg506X/Arg506X} group. In the PAT, the latency time of the *Atp6v1b2*^{Arg506X/Arg506X} and *Atp6v1b2*^{Arg506X/+} mice did not differ significantly between the three days, which was different with WT mice, indicating that WT mice had established the association between foot shock and entering the dark compartment but mutant mice were unable to establish the association.

To examine anxiety-related behavior, an open-field test, elevated plus maze test and light-dark exploration test were performed. However, there was no increased anxiety-related behavior in *Atp6v1b2*^{Arg506X/+} or *Atp6v1b2*^{Arg506X/Arg506X} mice.

In addition, the MWM test failed to proceed due to the epileptic symptom in *Atp6v1b2*^{Arg506X/Arg506X} mice when they were placed into water (Fig. 4c, Supplementary Movie).



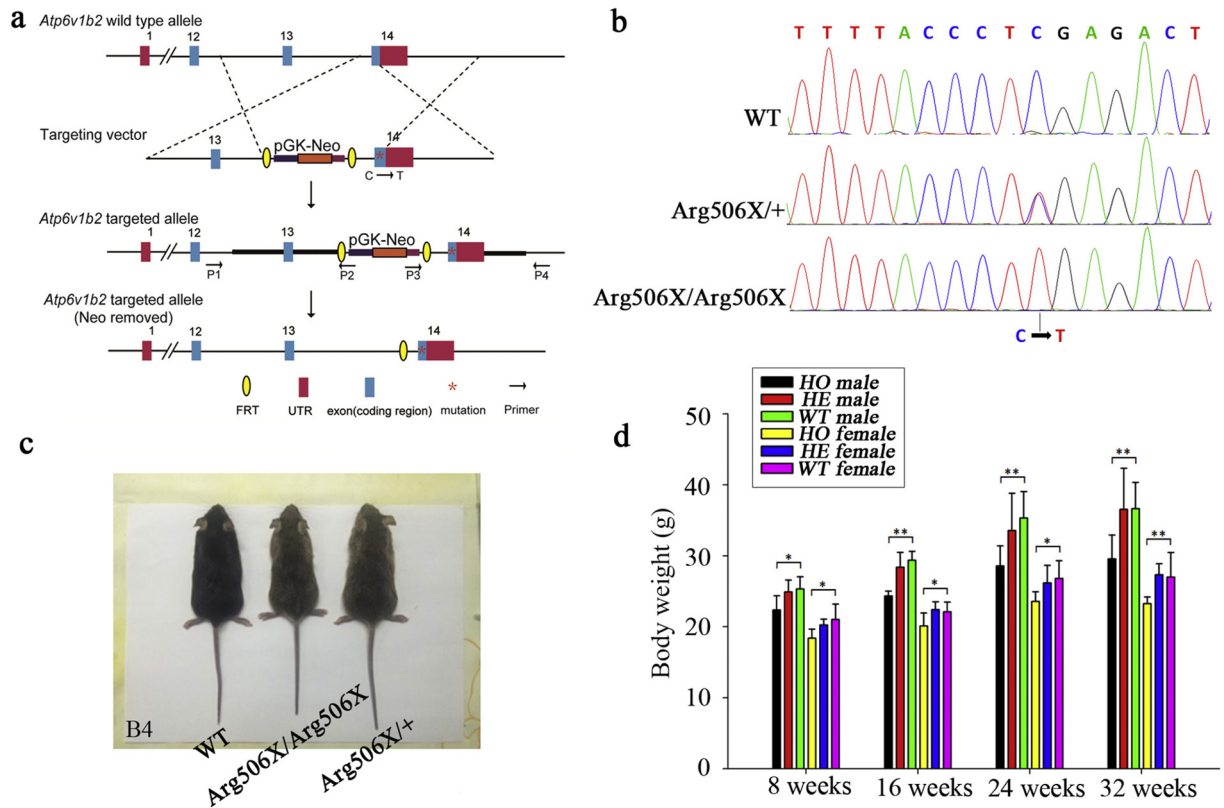


Fig. 2. General appearance of *Atp6v1b2* c.1516C>T knockin mice. (a) Targeted knockin of the *Atp6v1b2* c.1516C>T mutation in mouse ES cells was shown and the ES cell screening element (Neo) was designed in intron 13. (b) WT and mutant mice were genotyped by PCR. Partial sequences of exon 14 showed the c.1516C>T mutation. (c) The difference of body size was visible between *Atp6v1b2*^{Arg506X/Arg506X}, *Atp6v1b2*^{Arg506X/+}, and WT littermates at 16 weeks. *Atp6v1b2*^{Arg506X/Arg506X} mice were smaller than *Atp6v1b2*^{Arg506X/+} and WT mice (with B5 paper as the background). (d) *Atp6v1b2*^{Arg506X/Arg506X} mice had significantly lower body weights than *Atp6v1b2*^{Arg506X/+} and WT mice, and the difference became more and more obvious with increasing age (*P*-value decreased) (**P* < 0.05, ***P* < 0.01, one-way ANOVA).

3.6. *Atp6v1b2* deficiency affects the structure and functional connections of the mouse brain

rsfMRI was used to evaluate FC in the mouse brain. Although anesthesia may affect FC [35], due to its several advantages including non-invasive character and correspondingly high temporal and spatial resolution, rsfMRI has been applied to study diseases in both human and rodent brains [36].

Voxel-based morphometry was used to determine differences, in terms of brain structural abnormalities, between WT and *Atp6v1b2*^{Arg506X/Arg506X} mouse on T2-weighted anatomical images. Gray matter density in the *Atp6v1b2*^{Arg506X/Arg506X} mouse brain was significantly lower than that in the control group in the regions highlighted in the three-dimensional (3D) rendered image (mainly in the temporal lobe, occipital lobe and cerebellum) (Fig. 5a). Moreover, there was a significant difference between the tissue-specific volume of the WT and *Atp6v1b2*^{Arg506X/Arg506X} mouse brains: WT mice have less cerebrospinal fluid but more gray matter and white matter than *Atp6v1b2*^{Arg506X/Arg506X} mice (Fig. 5b).

FCs between regions of interest (27 on each hemisphere) were shown by correlation matrices. Several connections were significantly affected in the mouse model (Fig. 5c). The following FCs of WT mice were stronger than those of *Atp6v1b2*^{Arg506X/Arg506X} mice: left olfactory

bulb - right medulla, left cerebral cortex - right medulla, left medulla - left amygdala, left epithalamus - right amygdala, right cerebral cortex - right medulla, right anterior commissure - right medulla, right medulla - right pons, and right medulla - right fasciculus retroflexus. The following FCs of WT mice were weaker than those of *Atp6v1b2*^{Arg506X/Arg506X} mice: left olfactory bulb - right olfactory bulb, and left substantia nigra - right mammillary body.

Additionally, a seed-based analysis was performed with the hippocampus or amygdala as seed regions and the cortex as target region (Fig. 5d). Compared to WT mice, significant increases in some FCs were observed in *Atp6v1b2*^{Arg506X/Arg506X} mice, and these FCs were shown as follows: bilateral amygdala - region of the right prefrontal cortex, left hippocampus - region of the right prefrontal cortex, and left hippocampus - region of the left temporal.

3.7. *Atp6v1b2* deficiency results in an impaired hippocampal CA1 region in mice

Considering the correlation between *ATP6V1B2* deficits and hippocampal-dependent cognitive impairment [27], we focused on the hippocampus, especially the CA1 region, which is particularly susceptible to adverse events, such as oxidative damage, amyloid plaque

Fig. 1. Phenotypes of *atp6v1b2* zebrafish morphants. (a) The zebrafish *atp6v1b2* gene was targeted by specific MO antisense to prevent proper splicing of exon 4 (E414-MO). Primers 2F and 5R interrogate the presence of wild type (non-mutant) transcripts or those in which intron4–5 has been inserted. Left: RT-PCR of *atp6v1b2* transcript from control-MO and E414-MO injected embryos 2 days after fertilization, demonstrating insertion of intron4–5. Right: Sanger sequencing of both the wild type band and the intron4–5 inserted band validating the wild type sequence and the intron4–5 inserted sequence. (b–e) Compared to WT embryos (*n* = 10 per group), *atp6v1b2* knockdown group showed decreased body length (b, black dotted line, 32 hpf), brain ventricle size (b, green area, 32 hpf), severe pericardial oedema (b, black arrow, 32 hpf), inhibited inflation of the swim bladder (c, red arrow, 5 dpf), shorter pectoral fins (d, blue bracket, 6 dpf), and decreased hair cells (e, white star target, 5 dpf). Scale bars represent 100 μ m. (hpf, hours post fertilization; dpf, days post fertilization).

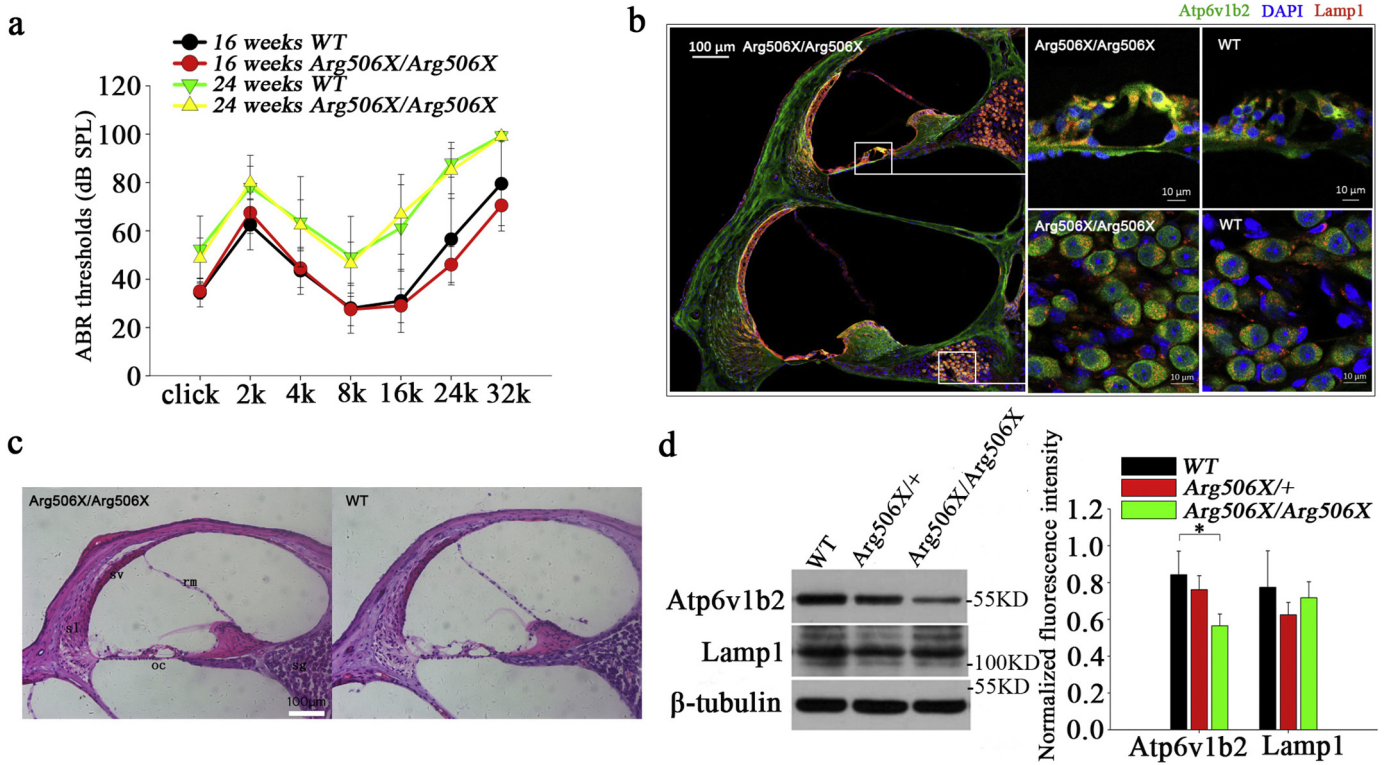


Fig. 3. Hearing and inner ear pathology in *Atp6v1b2* c.1516C > T knockin mice. (a) At 16 weeks and 24 weeks, the difference in mean ABR thresholds between *Atp6v1b2*^{Arg506X/Arg506X} and WT mice exposed to broadband click and pure tone frequencies of 2, 4, 8, 16, and 32 kHz was not statistically significant for either the click or pure tone stimulus (16 weeks: n = 10/group; 24 weeks: Arg506X/Arg506X: n = 11, WT: n = 8; P > 0.05, Student's t-test; n = number of test ears). (b) Immunofluorescence (at 16 weeks): *Atp6v1b2* (green, 488) existed in both WT and *Atp6v1b2*^{Arg506X/Arg506X} mice and expressed mainly in Corti organ (especially inner hair cells) and spiral ganglion. No abnormal expression of Lamp1 (red, 568) occurred in *Atp6v1b2*^{Arg506X/Arg506X} cochleas. (c) Hematoxylin and eosin staining (at 24 weeks): the morphologic analysis of the cochlea was normal (co: Corti organ, sg: spiral ganglion, rm: reissner's membrane, sv: stria vascularis, sl: spiral ligament). (d) Western blot (at 16 weeks): *Atp6v1b2* in *Atp6v1b2*^{Arg506X/Arg506X} cochlea was significantly less than that in WT and *Atp6v1b2*^{Arg506X/+} cochleas (*P < 0.05, one-way ANOVA). Lamp1 expression in the cochlea did not differ significantly between the three groups (P > 0.05, one-way ANOVA).

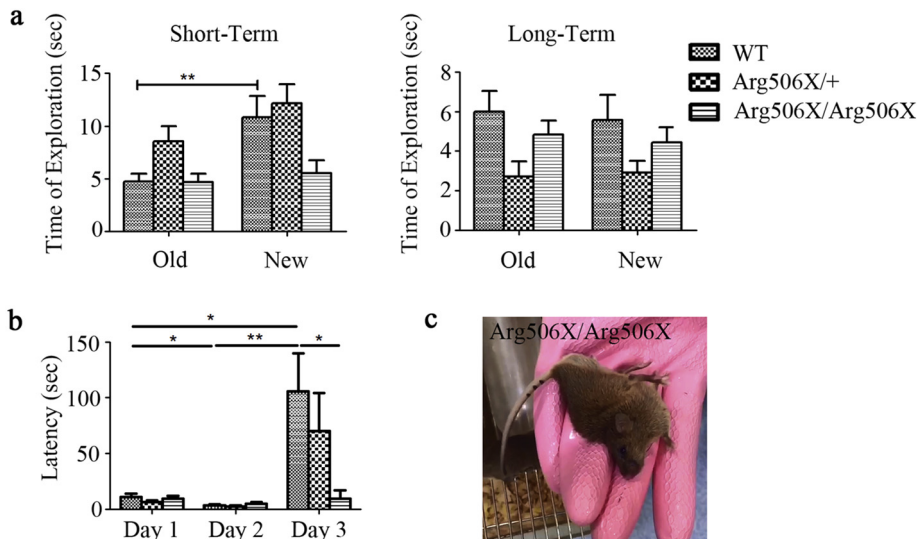


Fig. 4. *Atp6v1b2* c.1516C > T causes behavioral deficits in mice. (a) NOR test. Left: In a short period, (Day 2), the time spent on exploring the new block was significantly longer than that spent on exploring the old block for WT group (**P < 0.01, Student's t-test). However, the *Atp6v1b2*^{Arg506X/+} and *Atp6v1b2*^{Arg506X/Arg506X} groups showed no difference in exploration time between the new and old blocks (P > 0.05, Student's t-test, WT, n = 10; Arg506X/+, n = 11; Arg506X/Arg506X, n = 9). Right: In a long period (Day 3), the time spent on exploring old or new blocks showed no difference (P > 0.05, Student's t-test) for either WT, *Atp6v1b2*^{Arg506X/+}, or *Atp6v1b2*^{Arg506X/Arg506X} mice. (b) PAT was used to examine learning and memory abilities. WT mice had a shorter latency time on day 2 compared to Day 1 (*P < 0.05, Student's t-test). After foot shock on Day 2, the latency time on Day 3 was longer than that on Day 2 (**P < 0.01, Student's t-test) and day 1 (*P < 0.05, Student's t-test). However, the latency time of *Atp6v1b2*^{Arg506X/Arg506X} and *Atp6v1b2*^{Arg506X/+} mice showed no significant difference among the three days (P > 0.05, Student's t-test). In addition, WT mice had a longer latency time on Day 3 than *Atp6v1b2*^{Arg506X/Arg506X} mice (*P < 0.05, Student's t-test). (c) *Atp6v1b2*^{Arg506X/Arg506X} mice had epilepsy in the MWM test.

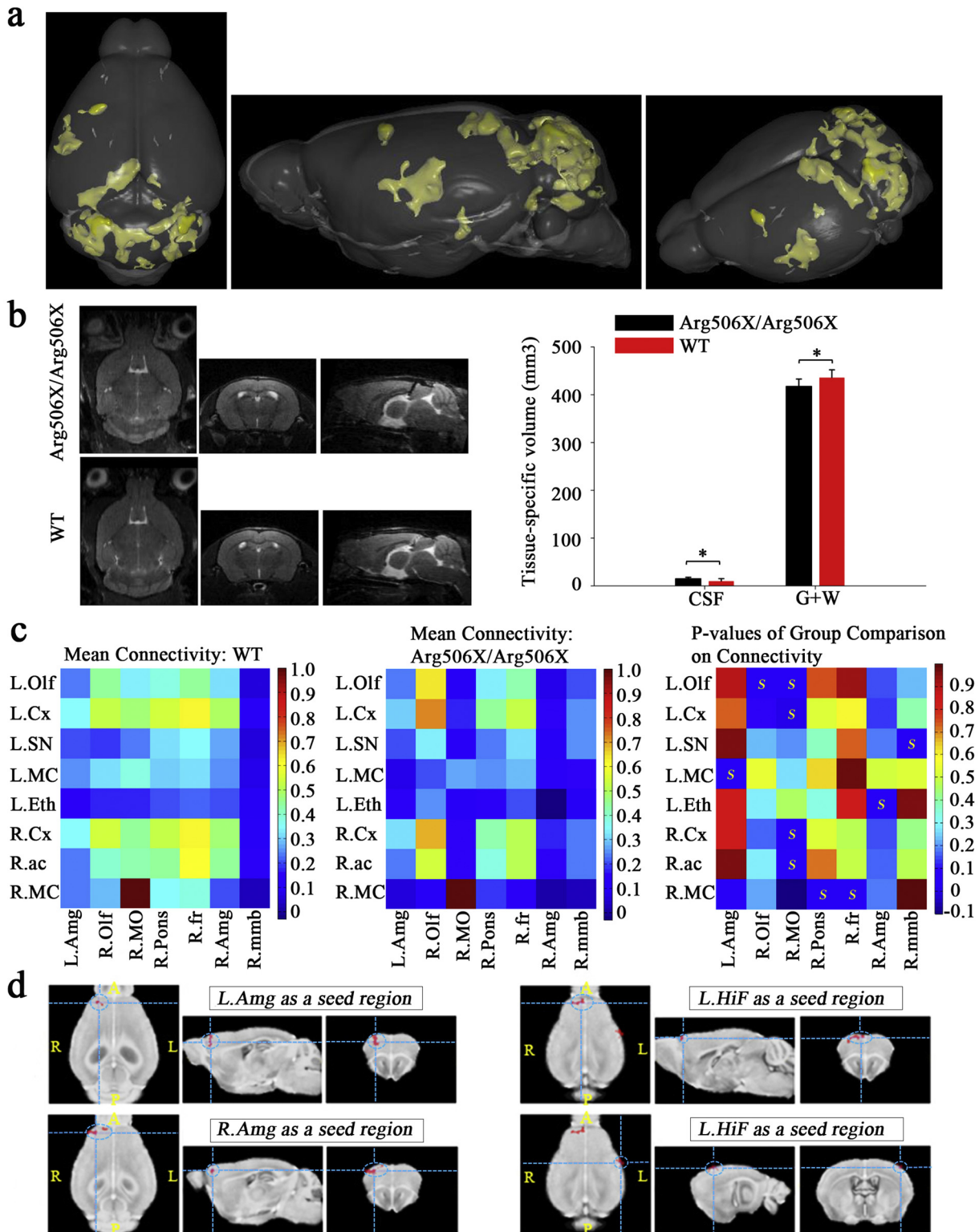


Fig. 5. Central nervous system abnormalities in *Atp6v1b2* c.1516C > T knockin mice by resting-state functional magnetic resonance imaging. (a) A three-dimensional (3D) rendering of regions with significant differences in gray matter density among groups was shown from different angles. Gray matter density in the *Atp6v1b2*^{Arg506X/Arg506X} mice brain was significantly lower than that in the WT mice brain in the regions highlighted ($P = 0.001$, Student's *t*-test, slice separation 200 μ m; cluster size threshold = 0.1 mm³). (b) Left: The T2-weighted anatomical images were shown (Left to right: horizontal, coronal and sagittal positions) and the cerebrospinal fluid (CSF) had a high signal. Right: The WT mice brain had smaller cerebrospinal fluid volume but larger gray matter and white matter (GM + WM) volume than the *Atp6v1b2*^{Arg506X/Arg506X} group (* $P < 0.05$, Student's *t*-test). (c) The z-transformed functional connection matrices of WT (left) and *Atp6v1b2*^{Arg506X/Arg506X} (middle) mice brain ($n = 7$ /group) were shown. The color scale represents the strength of the functional connection. *P*-values representing the difference between the WT and *Atp6v1b2*^{Arg506X/Arg506X} groups that can be visualized in a color map (right), and higher *P*-values are represented by warmer colors (Student's *t*-test). The regions where the WT group showed stronger connections than the *Atp6v1b2*^{Arg506X/Arg506X} group were as follows: L. Olf - R. MO; L. MO - L. Amg; L. Eth - R. Amg; R. Cx - R. MO; R. ac - R. MO; R. MO - R. Pons; R. MO - R. fr. The regions where the *Atp6v1b2*^{Arg506X/Arg506X} group showed stronger connections than the WT group were as follows: L. Olf - R. Olf; L. SN - R. MMB. (d) Group differences in the functional connections between the seed regions (hippocampus and amygdala) and target region (cortex) were analyzed. The target regions were marked by dotted lines. The seed - target regions that the *Atp6v1b2*^{Arg506X/Arg506X} group showed stronger connections than WT group were as follows: Amg on both sides - L. fra; L. HiF - L. fra/R. s1 ($p = 0.01$, Student's *t*-test, cluster size threshold = 0.1 mm³). Abbreviations: Olf = olfactory bulb, MO = medulla, Cx = cerebral cortex, Amg = amygdala, Eth = epithalamus, ac = anterior commissure, Pons = pons, fr = fasciculus retroflexus, HiF = hippocampal formation, fra = frontal association cortex, s1 = primary somatosensory cortex, Mmb = mammillary body, Sn = substantia nigra.

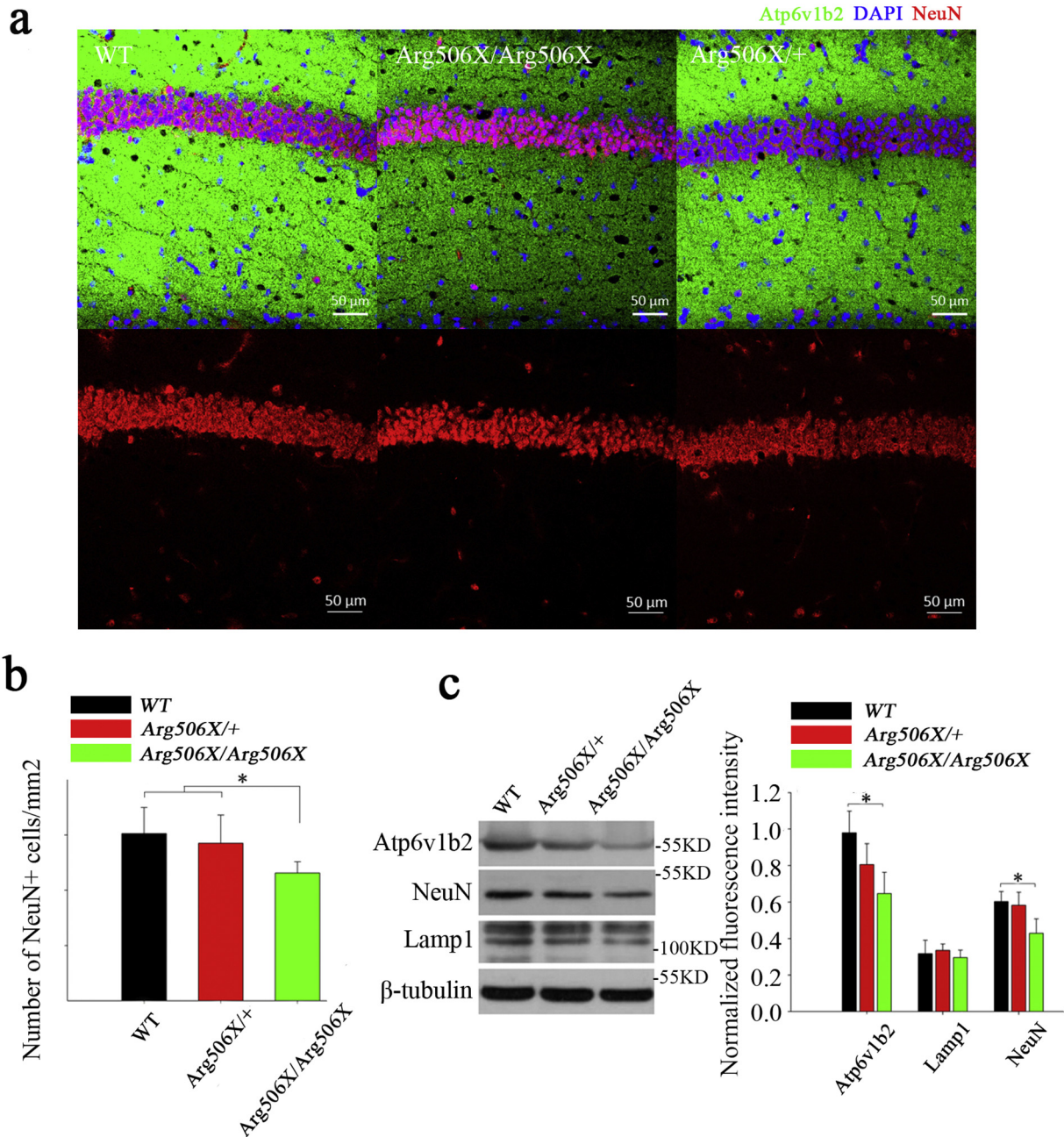


Fig. 6. *Atp6v1b2* deficiency results in an impaired CA1 region in mice. (a) Weaker fluorescence intensity of Atp6v1b2 was observed in the *Atp6v1b2*^{Arg506X/Arg506X} mice compared to the WT and *Atp6v1b2*^{Arg506X/+} mice as assessed by immunofluorescence. (b) The number of NeuN⁺ cells in the hippocampal CA1 region of *Atp6v1b2*^{Arg506X/Arg506X} mice was lower than that of WT and *Atp6v1b2*^{Arg506X/+} mice (**P* < 0.05, one-way ANOVA); (c) Atp6v1b2 and NeuN expressions in the *Atp6v1b2*^{Arg506X/Arg506X} hippocampus were significantly less than those in WT and *Atp6v1b2*^{Arg506X/+} mice, as assessed by Western blot (**P* < 0.05, one-way ANOVA).

deposition, ischemia, and memory impairments associated with aging [37,38]. Immunofluorescence and Western blot analysis were performed using the hippocampus tissue from adult mice (Fig. 6a). The number of mature neurons in the hippocampal CA1 region significantly decreased in *Atp6v1b2*^{Arg506X/Arg506X} mice (Fig. 6b). The number of NeuN⁺ cells (red, 568) in the hippocampal CA1 region of *Atp6v1b2*^{Arg506X/Arg506X} mice was less than that of WT and *Atp6v1b2*^{Arg506X/+} mice (*P* < 0.05, one-way ANOVA), and Atp6v1b2 (green, 488) was less abundant in the hippocampal CA1 region of *Atp6v1b2*^{Arg506X/Arg506X} mice than in WT and *Atp6v1b2*^{Arg506X/+} mice. Consistent with the immunofluorescence results, Atp6v1b2 and NeuN were significantly less abundant in the *Atp6v1b2*^{Arg506X/Arg506X} hippocampus than in the WT and *Atp6v1b2*^{Arg506X/+} hippocampus, according to Western blot analysis (*P* < 0.05, one-way ANOVA) (Fig. 6c).

3.8. *Atp6v1b2* c.1516C > T (p.Arg506X) weakly interacts with the E subunit

Since the B subunit is critical for the stability of V-ATPases, we examined the assembly of the V1 complex as a potential molecular mechanism of pump dysfunction. We precipitated Atp6v1b2 with the antibody to protein Atp6v1b2 on magnetic beads, and the protein that binds to Atp6v1b2 can also be precipitated such as Atp6v1e2. Through co-immunoprecipitation, both WT and mutant subunit B2 co-immunoprecipitated with the V1A and V0b subunits, demonstrating that *Atp6v1b2* c.1516C > T (p.Arg506X) had an intact V-ATPases assembly (Fig. 7a). C-terminal residues of the B subunit are important for the interaction with the E subunit [13]. Therefore, we examined the interaction between the B2 and V1E subunits by means of co-immunoprecipitation. As expected, the interaction with the E subunit

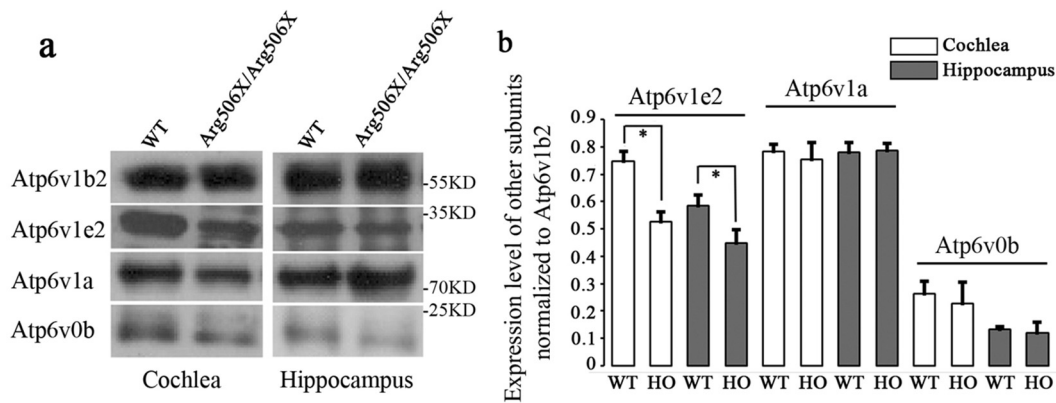


Fig. 7. The molecular mechanism involves a weak interaction between the E and B2 subunits. (a) Co-immunoprecipitation in both the hippocampus and cochlea of *Atp6v1b2* c.1516C > T knockin mice (16 weeks) was shown. (b) The normalized fluorescence intensities were compared between *Atp6v1b2*^{Arg506X/Arg506X} and WT groups by Student's t-test. Mutant subunit B2 co-immunoprecipitated with the V1E, V1A, or V0b subunit. However, the interaction between the E and B2 subunits was weaker than that of WT. With equal amount of Atp6v1b2, less binding with Atp6v1e2 was shown in *Atp6v1b2*^{Arg506X/Arg506X} mice than in WT mice (*P < 0.05, Student's t-test).

was weaker in *Atp6v1b2*^{Arg506X/Arg506X} mice than in WT mice (Fig. 7b). It is to be noted that in Fig. 3 and Fig. 5 (Western blot analysis), we used β -tubulin as the reference protein to eliminate errors caused by the sample amount, and the level of Atp6V1b2 in *Atp6v1b2*^{Arg506X/Arg506X} mice was significantly lower than that in WT mice. In Fig. 7, we used Atp6v1b2 as the reference to analyse the level of protein that bound to Atp6v1b2. However, the level of Atp6v1b2 was lower in *Atp6v1b2*^{Arg506X/Arg506X} mice than that in WT mice. Thus, we adjusted the amount of samples to ensure that the level of the reference protein–Atp6v1b2 was equal between the *Atp6v1b2*^{Arg506X/Arg506X} and WT groups; thus, the results more intuitively indicate the interaction between Atp6v1b2 and other subunits such as Atp6v1e2.

4. Discussion

ATP6V1B2 pathogenic variants lead to V-ATPases dysfunction and abnormal lysosome acidification, and underlie the molecular pathogenesis of DDOD syndrome and ZLS. Intelligence deficits are rarely reported in DDOD syndrome but are common in ZLS [22,24]. According to previous studies, patients with DDOD syndrome do not show obvious CNS disorders, while deafness may interfere with the diagnosis of preexisting mild cognitive problems [23]. It is possible that original mild CNS disorders exist in DDOD syndrome.

ATP6V1B2 is widely expressed throughout the body. Therefore, we explored the effect of mutant ATP6V1B2 on multiple organs and systems. The zebrafish is an excellent model of vertebrate embryonic development, and for the genetic analysis of such development. *Atp6v1b2* and its isoform, *atp6v1b1* (also termed vatB1), are expressed at all developmental stages of the zebrafish [39]. The two isoforms can be found in various tissues of adult zebrafish, including the gills, heart, liver, spleen, kidney, intestine, swim bladder, and muscle [40]. In the present work, *atp6v1b2*-knockdown zebrafish showed obvious hair cell loss, as expected. Zebrafish fins and tetrapod limbs are homologous in the context of early patterning and gene expression [41]. Thus, shortening of the pectoral fins in *atp6v1b2*-knockdown zebrafish indirectly supports that the gene is involved in the development of tetrapod limbs. Brain ventricles form the circulatory system in the brain. Abnormal brain ventricle size and development are associated with various neurodevelopmental disorders [42,43]. *Atp6v1b2*-knockdown zebrafish had a smaller brain ventricle size, supporting impaired neurodevelopment. Moreover, abnormal circulation in zebrafish may also contribute to subsequent reduction of the brain ventricles [44]. Phenotypic analysis of *atp6v1b2*-knockdown zebrafish suggested that *atp6v1b2* plays important roles in the development of multiple organs and systems.

Atp6v1b2 c.1516C > T knockin mouse model was created to elucidate the impact of the c.1516C > T variant, especially its effect on the CNS. In the present work, several behavioral tests (the NOR test, PAT, open-field test, elevated plus maze, light-dark exploration test, and MWM test) were used to investigate various behavioral and cognitive domains relevant to *Atp6v1b2* c.1516C > T knockin mouse model. *Atp6v1b2*^{Arg506X/Arg506X} mice showed obvious deficits in the NOR test and PAT. The NOR test measures recognition memory and has been extensively used in rodents [45]. In the NOR test, recognition of the features of different objects at the same location is supported by the perirhinal cortex and hippocampus [46]. The perirhinal cortex provides information on the novelty or familiarity of stimuli to the hippocampus. Moreover, there exists an anatomic relationship between the perirhinal cortex and the CA1 region of the hippocampus [47,48]. The PAT was established based on a rodent's preference for darkness and the fear memory of foot shocks; mice learn to avoid a dark compartment where they receive foot shocks. The PAT mainly reflects the function of the hippocampus and amygdala. The hippocampus governs declarative learning, while the amygdala is in charge of emotional processing [49]. In addition, the observation of epilepsy in *Atp6v1b2*^{Arg506X/Arg506X} mice in the MWM test indicates an association between *Atp6v1b2* and epilepsy. According to our observations of mice in the breeding process, the *Atp6v1b2*^{Arg506X/Arg506X} mice did not exhibit spontaneous seizures in their daily lives. However, the MWM test can induce epilepsy which seemed to be related to scare. Moreover, epilepsy also seemed to be related to temperature changes (when *Atp6v1b2*^{Arg506X/Arg506X} mice were placed into cold conditions, seizures occurred). According to previous studies, the expression of ATP6V1A and ATP6V1B2 both increased with neuronal maturation and synaptogenesis, indicating relationships between synaptogenesis and the two subunits. Defective ATP6V1A was found to lead to developmental encephalopathy with epilepsy, and the pathomechanism was reported to involve perturbations of lysosomal homeostasis and neuronal connectivity [50]. For mutant ATP6V1B2, it is possible that the synapse function is also impaired. Moreover, V-ATPase dysfunction may impact the synaptic vesicles and cause epilepsy considering its important roles in driving neurotransmitter loading into synaptic vesicles [51]. The epilepsy in the *Atp6v1b2* c.1516C > T knock-in mouse model requires further study.

Through voxel-based morphometry analysis of T2-weighted anatomical images, *Atp6v1b2*^{Arg506X/Arg506X} mouse brain structural abnormalities were observed: low gray matter density in some regions of the *Atp6v1b2*^{Arg506X/Arg506X} mouse brain (temporal lobe, occipital lobe, and cerebellum), less gray matter and white matter, and more cerebrospinal fluid than the WT mouse brain suggest abnormal brain development. Moreover, several FCs were significantly affected in the *Atp6v1b2*^{Arg506X/Arg506X} mouse brain according to rsfMRI, suggesting

deficits in related brain regions. Most of the related brain regions play important roles in learning and memory ability, including the olfactory bulb, amygdala and mammillary body [52–54]. Additionally, FC between the hippocampus or amygdala (seed regions) and target regions in the prefrontal cortex increased significantly in the *Atp6v1b2*^{Arg506X/Arg506X} mouse brain, corresponding to the compensatory increases in connectivity in the frontal cortex that occur early in cognitive disorders [55]. Together, these data suggest that the *Atp6v1b2* c.1516C > T leads to CNS impairments in mice.

As a highly vulnerable area, defects in the CA1 region of the hippocampus are associated with learning and memory impairment [46,56]. Moreover, the *ATP6V1B2* rs1106634 A allele is implicated in long-term memory deficits, which corresponds to the deficits observed in our behavioral tests [27]. It is possible that the CA1 region of the hippocampus is more sensitive to the functional impact of the c.1516C > T variant. As expected, we demonstrated that *Atp6v1b2* protein is expressed less in the hippocampus, and that the number of NeuN⁺ cells at CA1 region was significantly decreased in *Atp6v1b2*^{Arg506X/Arg506X} mice based on immunofluorescence and Western blot analysis. The impaired CA1 region of the hippocampus may be the pathological basis of the behavioral defects observed in *Atp6v1b2*^{Arg506X/Arg506X} mice.

The pathogenic variant *Atp6v1b2* c.1516C > T has been proven to cause V-ATPases dysfunction and abnormal acidification in lysosomes, but how V-ATPases is affected remains unknown [22]. Several studies have demonstrated that the B subunit is critical for stability of the V-ATPases. Disruption of the binding between the B1 subunit N-terminus and aldolase leads to impaired assembly of the V1 subcomplex [14]. Moreover, truncation of the B1 subunit C-terminus can also disrupt V1 assembly, affect the interaction with the E subunit and impair ATPases function [13]. A previous study predicted that mutant B2 (p.Arg485Pro) perturbs interactions within the V1 subcomplex according to protein structure analysis [24]. c.1516C > T (p.Arg506X) affects the same protein region and predicts a loss of the salt bridge between p.Tyr504 and p.Asp507 and a perturbing effect on V1 subcomplex assembly [22]. As expected, the interaction with the E subunit was weak compared to WT, which may influence the function of V-ATPases. However, assembly of V-ATPases still occurred even in the presence of mutant B2. Misfolded or damaged proteins will be degraded in cells, which likely reduced mutant B2 subunit expression in Western blot and immunofluorescence analysis.

Although the precise molecular mechanisms remain to be clarified, here, we explored the possible signalling pathways. In our study, defective *Atp6v1b2* weakly interacted with the E subunit and thus caused V-ATPase dysfunction. According to a previous study, inhibition of the V-ATPase can lead to downregulation of important signalling pathways such as Notch [57] and Wnt [58]. Postnatal dysregulation of Notch signalling was found to disrupt dendrite development by reducing the mTOR signalling pathway, thus leading to cognitive impairments [59]. Wnt signalling can be blocked by the Wnt inhibitor Dkk-1. One study has shown that mice that received Dkk-1 exhibited impaired novel object recognition memory [60]. In another study, mice in which canonical Wnt signalling was blocked by Dkk-1 in the amygdala showed impaired fear memory formation [61]. In our study, both the New Object Recognition Test (NOR) and Passive Avoidance Test (PAT) were performed in the *Atp6v1b2* c.1516C > T knock-in mouse model, and the results fit well with those of the two previous studies. Therefore, we hypothesised that the morphological changes are associated with the reduction in the Wnt signalling pathway.

Interestingly, *Atp6v1b2* c.1516C > T knockin mice with cognitive defects exhibited normal hearing and cochlear morphology under optical microscope in this study. The difference of hearing loss phenotype between human and mice may be due to a genetic compensation effect in mice which we are exploring to verify in the near future. There are several possible explanations for the hearing phenotype in *Atp6v1b2* c.1516C > T knockin mice. First, *Atp6v1b2*^{Arg506X/Arg506X} mice display normal hearing under normal conditions, but may develop hearing

impairments under unfavorable situations, such as aging and noise exposure, which requires further study. Second, other H⁺ exchangers, such as Na⁺/H⁺ and Cl⁻/H⁺ exchangers, may compensate for V-ATPases dysfunction [62]. Third, genetic buffering is believed to be a factor in our mouse model. Genetic compensation can be induced by deleterious mutations, but not gene knockdown [63]. Actually, both cochlea-specific *Atp6v1b2* knockdown mouse [22] and *atp6v1b2* knockdown zebrafish showed abnormal hearing with hair cell degeneration. Most subunits composing the V-ATPases have several isoforms expressed in different tissues, and isoform complementation has already emerged, including that of subunit B [21,64,65]. B2 subunit can substitute B1 subunit function by relocalizing B2-containing V-ATPases and thus *Atp6v1b1*^{-/-} mice showed normal hearing [21]. It is possible that *Atp6v1b1* compensates for the function of *Atp6v1b2*, as it is the homologous gene of *Atp6v1b2*. *Atp6v1b1* is mainly expressed in the kidney, epididymis, eyes, and inner ears, and no expression was detected in the brain [66], which may explain the phenomenon that the CNS disorders still occurred in our mouse model. In the *Atp6v1b2* c.1516C > T knockin mouse model, it is possible that compensation of the tissue-specific B1 subunit and brain vulnerability result in compensation in the cochlea but not the CNS; however, whether and how compensation buffering affects hearing impairment requires further investigation. The fact that *Atp6v1b2* c.1516C > T knockin mice with normal hearing exhibit cognitive problems supports preexisting CNS disorders in patients with DDOD syndrome.

This study had several limitations. First, systematic CNS evaluations in patients with DDOD are unavailable because of 1) the high heterogeneity of clinical manifestation and lack of an evaluation test for mild CNS disorders in patients in early childhood with severe hearing loss and 2) rsfMRI examinations could not be performed in patients with cochlear implants, and thus, further brain functional analysis was not possible. To address this issue, the long-term follow-up of patients with DDOD syndrome concerning the CNS disorders has been scheduled. Second, there is the possibility that there is late-onset hidden hearing loss in the *Atp6v1b2*^{Arg506X/Arg506X} mice older than 24 weeks, and we will closely examine the hearing in the mouse model. Third, different hearing phenotypes were identified in humans and the mutant mice with the same variant. We propose that there might be a certain compensation mechanism in the mouse model, which needs further clarification.

5. Conclusions

In summary, we created two genetic models and verified that a defect in *atp6v1b2* causes CNS disorders. Phenotypic analysis of the zebrafish model suggests that *atp6v1b2* impairment affects early development. The fact that *Atp6v1b2* c.1516C > T knockin mice exhibit decreased expression of *Atp6v1b2*, despite their normal hearing and cochlear morphology, suggests the existence of a compensatory mechanism in the inner ear, although this requires further investigation. Additionally, the impaired hippocampal CA1 region may be the pathological basis of the behavioral defects seen in *Atp6v1b2*^{Arg506X/Arg506X} mice. The molecular mechanism underlying V-ATPases dysfunction involves a weak interaction between the E and B2 subunits, although the assembly of V-ATPases can still take place.

Supplementary data to this article can be found online at <https://doi.org/10.1016/j.ebiom.2019.06.035>.

Funding

This study was supported by National Key Research and Development Project of China (2016YFC1000706), National Natural Science Foundation of China (81873704), and Fostering Funds of Chinese PLA General Hospital for National Distinguished Young Scholar Science Fund (2017-JQPY-001) to Yongyi Yuan. National Key Research and Development Project (2016YFC1000700, 2016YFC1000704), National

Natural Science Foundation of China (81730029, 61827805) and Beijing Natural Science Foundation (19G10054) to Pu Dai. National Natural Science Foundation of China (81770992, 81470683) to Weijiu Han. National Natural Science Foundation of China (81570929) and Beijing Natural Science Foundation (7192234) to Xue Gao. The funders had no role in study design, data collection and analysis, decision to publish, or preparation of the manuscript.

Availability of data and material

All data are presented in the manuscript or Additional files.

Author contributions

Weihao Zhao and Yongyi Yuan drafted the manuscript. Weihao Zhao and Shiwei Qiu participated in the construction and analysis of *Atp6v1b2* c.1516C>T knockin mice. Xue Gao participated in the construction and analysis of *atp6v1b2* knockdown zebrafish. Bo Gao and Song Gao participated in the following-up of patients. Dongyang Kang and Xin Zhang participated in the molecular biology experiment. Yongyi Yuan, Weijiu Han and Pu Dai conceived the study, participated in its design and coordination. All authors have read and approved the final manuscript.

Declaration of Competing Interests

The authors declare that they have no competing interests.

Consent for publication

We have obtained consents to publish this paper from all the participants of this study.

Ethics approval

This study was approved by the Ethics Committee of the Chinese People's Liberation Army General Hospital (reference number S2016-120-02).

Acknowledgements

We sincerely thank all the family members for their participation and cooperation in this study.

References

- [1] Beyenbach KW, Wieczorek H. The V-type H⁺ ATPase: molecular structure and function, physiological roles and regulation. *J Exp Biol* 2006;209(Pt 4):577–89.
- [2] Smardon AM, Tarsio M, Kane PM. The RAVE complex is essential for stable assembly of the yeast V-ATPase. *J Biol Chem* 2002;277(16):13831–9.
- [3] Zhao J, Benlekbir S, Rubinstein JL. Electron cryomicroscopy observation of rotational states in a eukaryotic V-ATPase. *Nature* 2015;521(7551):241–5.
- [4] Mindell JA. Lysosomal acidification mechanisms. *Annu Rev Physiol* 2012;74:69–86.
- [5] Schoonderwoert VT, Martens GJ. Targeted disruption of the mouse gene encoding the V-ATPase accessory subunit Ac45. *Mol Membr Biol* 2002;19(1):67–71.
- [6] Marshansky V, Futai M. The V-type H⁺-ATPase in vesicular trafficking: targeting, regulation and function. *Curr Opin Cell Biol* 2008;20(4):415–26.
- [7] Poëa-Guyon S, Ammar MR, Erard M, et al. The V-ATPase membrane domain is a sensor of granular pH that controls the exocytotic machinery. *J Cell Biol* 2013;203(2):283–98.
- [8] Colacurcio DJ, Nixon RA. Disorders of lysosomal acidification—the emerging role of v-ATPase in aging and neurodegenerative disease. *Ageing Res Rev* 2016;32:75–88.
- [9] Van Damme T, Gardeitchik T, Mohamed M, et al. Mutations in ATP6V1E1 or ATP6V1A cause autosomal-recessive cutis laxa. *Am J Hum Genet* 2017;100(2):216–27.
- [10] Ajmal M, Mir A, Wahid S, et al. Identification and in silico characterization of a novel p.P208PfsX1 mutation in V-ATPase a3 subunit associated with autosomal recessive osteopetrosis in a Pakistani family. *BMC Med Genet* 2017;18(1):148.
- [11] Stransky L, Cotter K, Forgac M. The function of V-ATPases in cancer. *Physiol Rev* 2016;96(3):1071–91.
- [12] Escobar LI, Simian C, Treard C, et al. Mutations in ATP6V1B1 and ATP6V0A4 genes cause recessive distal renal tubular acidosis in Mexican families. *Mol Genetics Genom* 2016;4(3):303–11.
- [13] Fuster DG, Zhang J, Xie XS, Moe OW. The vacuolar-ATPase B1 subunit in distal tubular acidosis: novel mutations and mechanisms for dysfunction. *Kidney Int* 2008;73(10):1151–8.
- [14] Lu M, Ammar D, Ives H, Albrecht F, Gluck SL. Physical interaction between aldolase and vacuolar H⁺-ATPase is essential for the assembly and activity of the proton pump. *J Biol Chem* 2007;282(34):24495–503.
- [15] Holliday LS, Lu M, Lee BS, et al. The amino-terminal domain of the B subunit of vacuolar H⁺-ATPase contains a filamentous actin binding site. *J Biol Chem* 2000;275(41):32331–7.
- [16] Wagner CA, Finberg KE, Breton S, Marshansky V, Brown D, Geibel JP. Renal vacuolar H⁺-ATPase. *Physiol Rev* 2004;84(4):1263–314.
- [17] Paunescu TG, Da Silva N, Marshansky V, McKee M, Breton S, Brown D. Expression of the 56-kDa B2 subunit isoform of the vacuolar H(+) -ATPase in proton-secreting cells of the kidney and epididymis. *Am J Physiol Cell Physiol* 2004;287(1):C149–62.
- [18] Pietrement C, Sun-Wada GH, Silva ND, et al. Distinct expression patterns of different subunit isoforms of the V-ATPase in the rat epididymis. *Biol Reprod* 2006;74(1):185–94.
- [19] Wax MB, Saito I, Tenkova T, et al. Vacuolar H⁺-ATPase in ocular ciliary epithelium. *Proc Natl Acad Sci U S A* 1997;94(13):6752–7.
- [20] Karet FE, Finberg KE, Nelson RD, et al. Mutations in the gene encoding B1 subunit of H⁺-ATPase cause renal tubular acidosis with sensorineural deafness. *Nat Genet* 1999;21(1):84–90.
- [21] Paunescu TG, Russo LM, Da Silva N, et al. Compensatory membrane expression of the V-ATPase B2 subunit isoform in renal medullary intercalated cells of B1-deficient mice. *Am J Physiol Renal Physiol* 2007;293(6):F1915–26.
- [22] Yuan Y, Zhang J, Chang Q, et al. De novo mutation in ATP6V1B2 impairs lysosome acidification and causes dominant deafness-onychodystrophy syndrome. *Cell Res* 2014;24(11):1370–3.
- [23] Menendez I, Carranza C, Herrera M, et al. Dominant deafness-onychodystrophy syndrome caused by an ATP6V1B2 mutation. *Clin Case Rep* 2017;5(4):376–9.
- [24] Kortum F, Caputo V, Bauer CK, et al. Mutations in KCNH1 and ATP6V1B2 cause Zimmermann-Laband syndrome. *Nat Genet* 2015;47(6):661–7.
- [25] Woody SK, Zhou H, Ibrahim S, Dong Y, Zhao L. Human ApoE varepsilon2 promotes regulatory mechanisms of bioenergetic and synaptic function in female brain: a focus on V-type H⁺-ATPase. *J Alzheimers Dis* 2016;53(3):1015–31.
- [26] Baulac S, Gourfinkel-An I, Couarch P, et al. A novel locus for generalized epilepsy with febrile seizures plus in French families. *Arch Neurol* 2008;65(7):943–51.
- [27] Gonda X, Eslzari N, Anderson IM, Deakin JF, Bagdy G, Juhász G. Association of ATP6V1B2 rs1106634 with lifetime risk of depression and hippocampal neurocognitive deficits: possible novel mechanisms in the etiopathology of depression. *Transl Psychiatry* 2016;6(11):e945.
- [28] Deal JA, Sharrett AR, Albert MS, et al. Hearing impairment and cognitive decline: a pilot study conducted within the atherosclerosis risk in communities neurocognitive study. *Am J Epidemiol* 2015;181(9):680–90.
- [29] Book WM. *The Zebrafish Book: A Guide for the Laboratory use of Zebrafish*. Eugene. The University of Oregon Press; 1993.
- [30] Kimmel CB, Ballard WW, Kimmel SR, Ullmann B, Schilling TF. Stages of embryonic development of the zebrafish. *Dev Dyn* 1995;203(3):253–310.
- [31] Nasevicius A, Ekker SC. Effective targeted gene 'knockdown' in zebrafish. *Nat Genet* 2000;26(2):216–20.
- [32] Liu P, Jenkins NA, Copeland NG. A highly efficient recombineering-based method for generating conditional knockouts. *Genome Res* 2003;13(3):476–84.
- [33] Cope EC, Opendak M, LaMarca EA, et al. The effects of living in an outdoor enclosure on hippocampal plasticity and anxiety-like behavior in response to nematode infection. *Hippocampus* 2019;29(4):366–77.
- [34] Mauvezin C, Nagy P, Juhász G, Neufeld TP. Autophagosome-lysosome fusion is independent of V-ATPase-mediated acidification. *Nat Commun* 2015;6:7007.
- [35] Grandjean J, Schroeter A, Batata I, Rudin M. Optimization of anesthesia protocol for resting-state fMRI in mice based on differential effects of anesthetics on functional connectivity patterns. *NeuroImage* 2014;102(Pt 2):838–47.
- [36] Ding X, Li CY, Wang QS, et al. Patterns in default-mode network connectivity for determining outcomes in cognitive function in acute stroke patients. *Neuroscience* 2014;277:637–46.
- [37] Wang X, Michaelis EK. Selective neuronal vulnerability to oxidative stress in the brain. *Front Aging Neurosci* 2010;2:12.
- [38] Burger C. Region-specific genetic alterations in the aging hippocampus: implications for cognitive aging. *Front Aging Neurosci* 2010;2:140.
- [39] Schredelseker J, Pelster B. Isoforms vatB1 and vatB2 of the vacuolar type ATPase subunit B are differentially expressed in embryos of the zebrafish (*Danio rerio*). *Dev Dyn* 2004;230(3):569–75.
- [40] Boesch ST, Eller B, Pelster B. Expression of two isoforms of the vacuolar-type ATPase subunit B in the zebrafish *Danio rerio*. *J Exp Biol* 2003;206(Pt 11):1907–15.
- [41] Ito T, Handa H. Deciphering the mystery of thalidomide teratogenicity. *Congenit Anom* 2012;52(1):1–7.
- [42] Eyles DW, Feron F, Cui X, et al. Developmental vitamin D deficiency causes abnormal brain development. *Psychoneuroendocrinology* 2009;34(Suppl. 1):S247–57.
- [43] Korzh V. Development of brain ventricular system. *Cell Mol Life Sci* 2018;75(3):375–83.
- [44] Lowery LA, Sive H. Initial formation of zebrafish brain ventricles occurs independently of circulation and requires the *nanog* and *atp1a1a.1* gene products. *Development* 2005;132(9):2057–67.
- [45] Grayson B, Leger M, Piercy C, Adamson L, Harte M, Neill JC. Assessment of disease-related cognitive impairments using the novel object recognition (NOR) task in rodents. *Behav Brain Res* 2015;285:176–93.

- [46] Cohen SJ, Munchow AH, Rios LM, Zhang G, Asgeirsdottir HN, Stackman Jr RW. The rodent hippocampus is essential for nonspatial object memory. *Curr Biol* 2013;23(17):1685–90.
- [47] Naber PA, Witter MP, Lopez da Silva FH. Perirhinal cortex input to the hippocampus in the rat: evidence for parallel pathways, both direct and indirect. A combined physiological and anatomical study. *Eur J Neurosci* 1999;11(11):4119–33.
- [48] Kinnavane L, Amin E, Olarte-Sanchez CM, Aggleton JP. Detecting and discriminating novel objects: the impact of perirhinal cortex disconnection on hippocampal activity patterns. *Hippocampus* 2016;26(11):1393–413.
- [49] Bechara A, Tranel D, Damasio H, Adolphs R, Rockland C, Damasio AR. Double dissociation of conditioning and declarative knowledge relative to the amygdala and hippocampus in humans. *Science* 1995;269(5227):1115–8.
- [50] Fassio A, Esposito A, Kato M, et al. De novo mutations of the ATP6V1A gene cause developmental encephalopathy with epilepsy. *Brain* 2018;141(6):1703–18.
- [51] Egashira Y, Takase M, Takamori S. Monitoring of vacuolar-type H⁺ ATPase-mediated proton influx into synaptic vesicles. *J Neurosci* 2015;35(8):3701–10.
- [52] Pena RR, Pereira-Caixeta AR, Moraes MF, Pereira GS. Anisomycin administered in the olfactory bulb and dorsal hippocampus impaired social recognition memory consolidation in different time-points. *Brain Res Bull* 2014;109:151–7.
- [53] Vann SD. Re-evaluating the role of the mammillary bodies in memory. *Neuropsychologia* 2010;48(8):2316–27.
- [54] Pape HC, Stork O. Genes and mechanisms in the amygdala involved in the formation of fear memory. *Ann N Y Acad Sci* 2003;985:92–105.
- [55] Damoiseaux JS, Prater KE, Miller BL, Greicius MD. Functional connectivity tracks clinical deterioration in Alzheimer's disease. *Neurobiol Aging* 2012;33(4) (828 e19–30).
- [56] Platano D, Fattoretti P, Baliotti M, et al. Synaptic remodeling in hippocampal CA1 region of aged rats correlates with better memory performance in passive avoidance test. *Rejuvenation Res* 2008;11(2):341–8.
- [57] Wissel S, Harzer H, Bonnay F, Burkard TR, Neumuller RA, Knoblich JA. Time-resolved transcriptomics in neural stem cells identifies a v-ATPase/notch regulatory loop. *J Cell Biol* 2018;217(9):3285–300.
- [58] Cruciat CM, Ohkawara B, Acebron SP, et al. Requirement of prorenin receptor and vacuolar H⁺-ATPase-mediated acidification for Wnt signaling. *Science* 2010;327(5964):459–63.
- [59] Ding XF, Gao X, Ding XC, Fan M, Chen J. Postnatal dysregulation of notch signal disrupts dendrite development of adult-born neurons in the hippocampus and contributes to memory impairment. *Sci Rep* 2016;6:25780.
- [60] Fortress AM, Schram SL, Tuscher JJ, Frick KM. Canonical Wnt signaling is necessary for object recognition memory consolidation. *J Neurosci* 2013;33(31):12619–26.
- [61] Maguschak KA, Ressler KJ. Wnt signaling in amygdala-dependent learning and memory. *J Neurosci* 2011;31(37):13057–67.
- [62] Xiong J, Zhu MX. Regulation of lysosomal ion homeostasis by channels and transporters. *Sci China Life Sci* 2016;59(8):777–91.
- [63] Rossi A, Kontarakis Z, Gerri C, et al. Genetic compensation induced by deleterious mutations but not gene knockdowns. *Nature* 2015;524(7564):230–3.
- [64] Murata Y, Sun-Wada GH, Yoshimizu T, Yamamoto A, Wada Y, Futai M. Differential localization of the vacuolar H⁺ pump with G subunit isoforms (G1 and G2) in mouse neurons. *J Biol Chem* 2002;277(39):36296–303.
- [65] Sun-Wada GH, Yoshimizu T, Imai-Senga Y, Wada Y, Futai M. Diversity of mouse proton-translocating ATPase: presence of multiple isoforms of the C, d and G subunits. *Gene* 2003;302(1–2):147–53.
- [66] Yue F, Cheng Y, Breschi A, et al. A comparative encyclopedia of DNA elements in the mouse genome. *Nature* 2014;515(7527):355–64.